Spin excitation anisotropy in the paramagnetic tetragonal phase of BaFe_{2}As_{2}

Yu Li, Weiyi Wang, Yu Song, Haoran Man, Xingye Lu, Frédéric Bourdarot, and Pengcheng Dai

Phys. Rev. B **96**, 020404 — Published 6 July 2017

DOI: 10.1103/PhysRevB.96.020404

Spin excitation anisotropy in the paramagnetic tetragonal phase of $BaFe_2As_2$

Yu Li,[1] Weiyi Wang,[1] Yu Song,[1] Haoran Man,[1] Xingye Lu,[2] Frédéric Bourdarot,[3] and Pengcheng Dai[1,2,*]

[1]*Department of Physics and Astronomy, Rice University, Houston, Texas 77005, USA*
[2]*Center for Advanced Quantum Studies and Department of Physics, Beijing Normal University, Beijing 100875, China*
[3]*Institut Laue Langevin, 71 Avenue des Martyrs, 38042 Grenoble, France*

(Dated: June 20, 2017)

We use neutron polarization analysis to study temperature dependence of the spin excitation anisotropy in $BaFe_2As_2$, which has a tetragonal-to-orthorhombic structural distortion at T_s and antiferromagnetic (AF) phase transition at T_N with ordered moments along the orthorhombic a-axis below $T_s \approx T_N \approx 136$ K. In the paramagnetic tetragonal state at 160 K, spin excitations are isotropic in spin space with $M_a = M_b = M_c$, where M_a, M_b, and M_c are spin excitations polarized along the a, b, and c-axis directions of the orthorhombic lattice, respectively. On cooling towards T_N, significant spin excitation anisotropy with $M_a > M_b \approx M_c$ develops below 3 meV with a diverging M_a at T_N. The in-plane spin excitation anisotropy in the tetragonal phase of $BaFe_2As_2$ is similar to those seen in the tetragonal phase of its electron and hole-doped superconductors, suggesting that spin excitation anisotropy is a direct probe of doping dependence of spin-orbit coupling and its connection to superconductivity in iron pnictides.

PACS numbers: 74.70.Xa, 75.30.Gw, 78.70.Nx

The iron pnictide superconductors have a rich phase diagram including an orthorhombic lattice distortion associated with ferro-orbital order and nematic phase, antiferromagnetic (AF) order, and superconductivity [1–6]. In the undoped state, a parent compound of iron pnictide superconductors $BaFe_2As_2$ forms stripe AF order at T_N near a tetragonal-to-orthorhombic structural transition temperature T_s [Fig. 1(a)] [7–9]. Superconductivity can be induced by partially replacing Ba by K in $BaFe_2As_2$ to form hole-doped $Ba_{1-x}K_xFe_2As_2$ or by partially replacing Fe by TM (TM =Co, Ni) to form electron-doped $BaFe_{2-x}TM_xAs_2$ [1–3]. Although much attention has been focused on understanding the interplay between magnetism and superconductivity in these materials [1–3], a more subtle and much less explored facet involves the effect of spin-orbit coupling (SOC) [10], which translates anisotropies in real space into anisotropies in spin space and determines the easy axis of the magnetic ordered moment [Fig. 1(b)], and its connection with the electronic nematic phase and superconductivity [5, 11]. Since a nematic quantum critical point is believed to occur near optimal superconductivity in electron and hole-doped iron pncitides [12], it is important to determine the temperature and electron/hole doping evolution of SOC and its association with the nematic phase and superconductivity.

One way to achieve this in iron pnictides is to study the energy, wave vector, temperature, and doping dependence of the spin excitation anisotropy using neutron polarization analysis. Compared with angle resolved photoemission experiments [10], polarized neutron scattering experiments typically have much better energy and momentum resolution [3]. In previous work on electron-doped $BaFe_{2-x}TM_xAs_2$ [13–16] and hole-doped $Ba_{1-x}K_xFe_2As_2$ iron pnictides [17–19], there are clear evidence for spin excitation anisotropy in the paramagnetic tetragonal phase with $M_a \approx M_c > M_b$, where M_a, M_b, and M_c are spin excitations polarized along the a, b, and c-axis directions of the AF orthorhombic lattice, respectively, at temperatures well above T_N and T_s [15, 19]. Although low-energy spin waves in the parent compound $BaFe_2As_2$ are also anisotropic in the orthorhombic AF ordered state with $M_c > M_b > M_a$ [20, 21], temperature dependence of the inelastic magnetic scattering at the AF ordering wave vector $\mathbf{Q}_{AF} = \mathbf{Q}_1 = (1, 0, 1)$ [Figs. 1(b) and 1(c)] and an energy transfer of $E = 10$ meV changes from isotropic to anisotropic on cooling below T_N [20]. However, the energy scale of isotropic paramagnetic scattering at $E = 10$ meV in $BaFe_2As_2$ is considerably larger than that of the anisotropic paramagnetic spin excitation in doped superconductors ($E < 6$ meV) [15–19]. Since the SOC-induced spin space anisotropy is present in the paramagnetic tetragonal phase of doped iron pnictide superconductors and is also expected to be present in undoped $BaFe_2As_2$, it is possible that paramagnetic spin excitations in $BaFe_2As_2$ are also anisotropic, but with an energy scale smaller than $E = 10$ meV.

To test if this is indeed the case, we carried out polarized neutron scattering experiments on $BaFe_2As_2$ with $T_N \approx T_s \approx 136$ K to study the temperature dependence of the spin excitation anisotropy [Fig. 1(d)]. In the AF ordered state at $T = 135$ K, we find $M_c > M_b > M_a$ at $\mathbf{Q}_{AF} = (1, 0, 1)$ [Figs. 2(a), 2(b), and 3(a)], confirming the earlier results at 10 K [20, 21]. On warming to $T = 138$ K ($> T_N, T_s$) in the paramagnetic tetragonal state, spin excitations at $\mathbf{Q}_{AF} = (1, 0, 1)$ are still anisotropic below $E = 4$ meV but with $M_a > M_b \approx M_c$ [Figs. 2(c), 2(d), and 3(b)]. For comparison, spin excitations at the AF zone boundary (ZB) $\mathbf{Q}_{ZB} = (1, 0, 0)$ are isotropic for energies above $E = 2$ meV [Fig. 3(d)]. Upon

further warming to $T = 160$ K, paramagnetic scattering becomes isotropic at all energies probed ($8 \geq E \geq 2$ meV) [Fig. 3(c)]. While temperature dependence of the spin excitations at $E = 8$ meV and $\mathbf{Q}_{AF} = (1, 0, 1)$ transforms from isotropic to anisotropic below T_N with no evidence of critical scattering consistent with earlier measurements at $E = 10$ meV [20], paramagnetic scattering at $E = 2$ meV starts to develop spin space anisotropy below about 160 K with enhanced M_a ($> M_b \approx M_c$) on approaching T_N due to condensation of the longitudinal component of the magnetic critical scattering into a-axis aligned AF Bragg peak below T_N [Fig. 4(a)-4(f)] [9]. On the other hand, paramagnetic scattering at $E = 2$ meV and $\mathbf{Q}_{ZB} = (1, 0, 0)$ is isotropic at all temperatures above T_N [Fig. 4(g)-4(h)]. By comparing these results with spin excitation anisotropy in the paramagnetic tetragonal phase of electron/hole doped iron pnictide superconductors [15–19], we conclude that electron/hole doping in $BaFe_2As_2$ necessary to induce superconductivity also enhances the c-axis polarized spin excitations associated with superconductivity. These results are also in line with the tetragonal $C4$ magnetic phase with spins aligned along the c-axis in near optimally hole doped superconducting $Ba_{1-x}K_xFe_2As_2$ [22–25].

Our polarized neutron scattering experiments were carried out using the IN22 triple-axis spectrometers at the Institut Laue-Langevin, Grenoble, France. Polarized neutrons were produced using a focusing Heusler monochromator and analyzed with a focusing Heusler analyzer with a final wave vector of $k_f = 2.662$ Å^{-1}. About 12-g single crystals of $BaFe_2As_2$ used in previous work [26] are used in the present experiment. Figure 1(a) shows the collinear AF structure of $BaFe_2As_2$ with ordered moments along the a-axis [7–9]. The orthorhombic lattice parameters of the AF unit cell are $a \approx b \approx 5.549$ Å, and $c = 12.622$ Å. The wave vector transfer $\mathbf{Q}$ in three-dimensional reciprocal space in Å^{-1} is defined as $\mathbf{Q} = H\mathbf{a}^* + K\mathbf{b}^* + L\mathbf{c}^*$, with $\mathbf{a}^* = \frac{2\pi}{a}\hat{\mathbf{a}}$, $\mathbf{b}^* = \frac{2\pi}{b}\hat{\mathbf{b}}$ and $\mathbf{c}^* = \frac{2\pi}{c}\hat{\mathbf{c}}$, where H, K and L are Miller indices. The samples were co-aligned in the $[H, 0, L]$ scattering plane [Figs. 1(b) and 1(c)]. In this notation, the AF Bragg peaks occur at $[1, 0, L]$ with $L = 1, 3, \ldots$, while the AF zone boundaries along the c-axis occur at $L = 0, 2, \ldots$. The magnetic responses at a particular $\mathbf{Q}$ along the a-, b-, and c-axis directions are marked as M_a, M_b, and M_c, respectively as shown in Fig. 1(b). In the paramagnetic tetragonal state, these correspond to magnetic excitations polarized along the in-plane longitudinal, in-plane transverse, and out-of-plane directions, respectively. The neutron polarization directions x, y, and z are defined as along $\mathbf{Q}$, perpendicular to $\mathbf{Q}$ but in the scattering plane, and perpendicular to both $\mathbf{Q}$ and the scattering plane, respectively [Fig. 1(c)]. From the observed neutron spin-flip (SF) scattering cross sections σ_x^{SF}, σ_y^{SF}, and σ_z^{SF}, we can calculate the components M_a, M_b, and M_c via $\sigma_x^{SF} = \frac{R}{R+1}(\sin^2\theta M_a + \cos^2\theta M_c) + \frac{R}{R+1}M_b + B$,

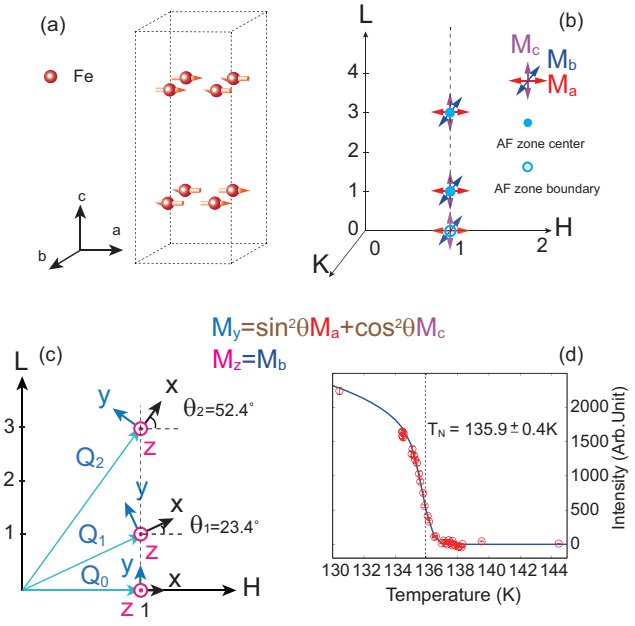

FIG. 1: (Color online) (a) The orthorhombic unit cell of $BaFe_2As_2$ (enclosed by dashed line) with only the magnetic Fe ions shown as red spheres. The arrows indicate the ordered moment direction along the longer a-axis. Along the c-axis the nearest neighboring spins are antiparallel. (b) The positions of reciprocal space probed in the present experiment. Magnetic fluctuations polarized along the a, b, and c directions are marked as M_a, M_b, and M_c, respectively. (c) Schematic of the $[H, 0, L]$ scattering plane, where wave vectors $\mathbf{Q}_0$, $\mathbf{Q}_1$, and $\mathbf{Q}_2$ are probed. The neutron polarization directions are along the x, y, and z. The angle between the x direction and H-axis is denoted as θ. (d) The temperature dependence of magnetic order parameter measured at $\mathbf{Q}_1 = (1, 0, 1)$. The solid line is a Gaussian convolved power law fit with $T_N = 135.9 \pm 0.4$ K.

$\sigma_y^{SF} = \frac{1}{R+1}(\sin^2\theta M_a + \cos^2\theta M_c) + \frac{R}{R+1}M_b + B$, and $\sigma_z^{SF} = \frac{R}{R+1}(\sin^2\theta M_a + \cos^2\theta M_c) + \frac{1}{R+1}M_b + B$, where R is the flipping ratio ($R = \sigma_{Bragg}^{NSF}/\sigma_{Bragg}^{SF} \approx 13$) and B is the background scattering. By measuring $\sigma_{x,y,z}^{SF}$ at two equivalent AF zone center wave vectors $\mathbf{Q}_{AF} = \mathbf{Q}_1 = (1, 0, 1)$ and $\mathbf{Q}_2 = (1, 0, 3)$, one can determine all three components of the magnetic response M_a, M_b, and M_c [15, 16, 19]. For the zone boundary position at $\mathbf{Q}_0 = (1, 0, 0)$ with $\theta = 0$, one can determine M_b and M_c using $\sigma_{x,y,z}^{SF}$ at this position.

To determine the magnetic ordering temperature of $BaFe_2As_2$, we show in Fig. 1(d) background subtracted elastic SF cross section σ_x^{SF} measured at $\mathbf{Q}_1 = (1, 0, 1)$. The solid line is a fit of the magnetic order parameter with Gaussian convolved power-law $M(T)^2 = B^2 \int (1 - \frac{T}{T_N})^{2\beta} e^{-(T-T_N)^2/2\sigma^2}$ [27]. Although this formula is used to account for sample inhomogeneities and a distribution of Néel temperatures in Co-doped $Ba(Fe_{1-x}Co_x)_2As_2$ [27], we use it for pure $BaFe_2As_2$, where disorder is not expected to be important, to compare with β and σ in

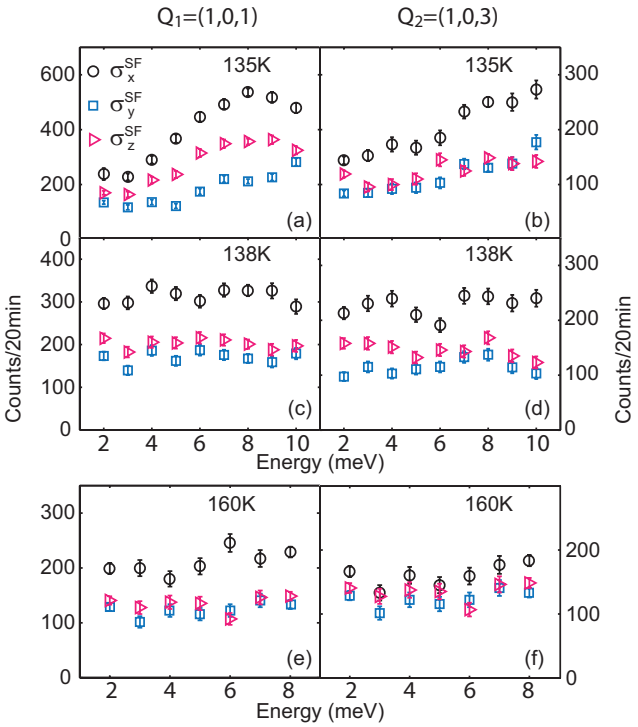

FIG. 2: (Color online) Constant-**Q** scans at the two AF wave vectors $\mathbf{Q}_1 = (1,0,1)$ and $\mathbf{Q}_2 = (1,0,3)$ at $T = 135$, 138, and 160 K. All three spin-flip (SF) channels σ_x^{SF}, σ_y^{SF}, σ_z^{SF} are measured at these wave vectors as defined in Fig.1 (c).

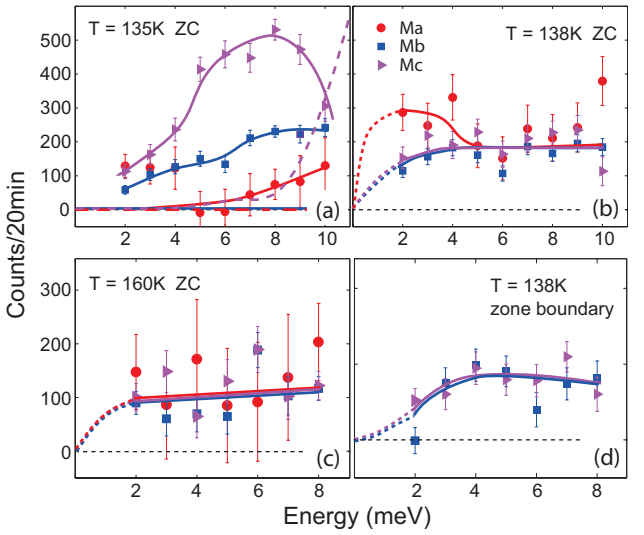

FIG. 3: (Color online) (a-c) The magnetic components M_a, M_b, and M_c at $\mathbf{Q}_{AF}$ and 135 K, 138 K, and 160 K obtained from data in Fig. 2. The dashed lines in (a) are results for spin waves of $BaFe_2As_2$ at 2 K [21]. (d) The magnetic components at the zone boundary (ZB) at 138 K. Only M_b and M_c can be determined from measurements at $\mathbf{Q} = (1,0,0)$.

lightly Co-doped samples. We find $T_N = 135.9 \pm 0.4$ K, $\sigma = 0.51 \pm 0.07$, and $\beta = 0.1 \pm 0.02$ for $BaFe_2As_2$. While the value of σ in $BaFe_2As_2$ is very similar to that of $x = 0.021$ suggesting a small distribution of T_N [27], the β value is considerably smaller than the Co-doped samples but similar to previous value of $\beta = 0.103$ for pure $BaFe_2As_2$ [30]. Figure 2 shows energy scans at the AF wave vectors $\mathbf{Q}_1 = (1,0,1)$ and $\mathbf{Q}_2 = (1,0,3)$ at temperatures below and above T_N. In an isotropic paramagnet with negligible background scattering and $R \to \infty$, we would expect $\sigma_x^{SF}/2 \approx \sigma_z^{SF} \approx \sigma_y^{SF}$. At $T = 135$ K below T_N, magnetic scattering at $\mathbf{Q}_1 = (1,0,1)$ shows strong anisotropy with $\sigma_z^{SF} > \sigma_y^{SF}$ [Fig. 2(a)]. Figure 2(b) plots similar scan at $\mathbf{Q}_2 = (1,0,3)$ with $\sigma_z^{SF} \approx \sigma_y^{SF}$. Since $\mathbf{Q}_1 = (1,0,1)$ and $\mathbf{Q}_2 = (1,0,3)$ correspond to angles of $\theta_1 = 23.4°$ and $\theta_1 = 52.4°$, respectively [Fig. 1(c)], we can use $\sigma_{x,y,z}^{SF}$ at these two wave vectors to completely determine M_a, M_b, and M_c [28, 29]. Figure 3(a) shows our calculated M_c, M_b, and M_a ($M_c > M_b > M_a$), and the outcome is similar to spin excitations of $BaFe_2As_2$ [21] and $BaFe_{1.91}Co_{0.09}As_2$ [16] in the low-temperature AF ordered phase.

In previous work, it was found that paramagnetic spin excitations of $BaFe_2As_2$ above T_N and T_s are isotropic at $E = 10$ meV and $\mathbf{Q}_1 = (1,0,1)$ [20]. To see if spin excitation anisotropy is present at $T = 138$ K ($> T_N, T_s$) in the paramagnetic tetragonal state, we carried out constant-**Q** measurements at $\mathbf{Q}_1$ [Fig. 2(c)] and $\mathbf{Q}_2$ [Fig. 2(d)]. Inspection of the figures finds clear difference in spin excitations ($\sigma_z^{SF} > \sigma_y^{SF}$) below about $E \approx 6$ meV at $\mathbf{Q}_2$. Figure 3(b) shows the energy dependence of M_a, M_b, and M_c obtained by using the data in Figs. 2(c) and 2(d), revealing $M_a > M_b \approx M_c$ for energies below 6 meV. Upon further warming the system to 160 K ($> T_N, T_s$), magnetic signal at $\mathbf{Q}_1$ [Figs. 2(e)] and $\mathbf{Q}_2$ [Figs. 2(f)] becomes purely paramagnetic isotropic scattering in the energy region probed satisfying $(\sigma_x^{SF} - B)/2 \approx (\sigma_y^{SF} - B) \approx (\sigma_z^{SF} - B)$. The energy dependence of M_a, M_b, and M_c shown in Fig. 3(c) confirm the isotropic paramagnetic nature of the scattering. Figure 3(d) shows the energy dependence of M_b and M_c as obtained from constant-**Q** scan at the zone boundary $\mathbf{Q}_0 = (1,0,0)$, indicating isotropic paramagnetic scattering at energies probed.

Figures 3(a)-3(c) summarize temperature evolution of the estimated M_a, M_b, and M_c at the AF zone center $\mathbf{Q}_{AF}$, obtained by using data in Fig. 2 after taking into account the magnetic form factor differences at $\mathbf{Q}_1$ and $\mathbf{Q}_2$ and other effects as shown in Ref. [29]. In the AF ordered state at $T = 135$ K ($\approx T_N - 1$ K), the M_c component dominates the spin excitation spectrum below 10 meV, followed by M_b and M_a [Fig. 3(a)]. For comparison, the M_a component of the spin waves is completely gapped out below ~10 meV at 2 K [dashed line in Fig. 3(a)]. When warming the system to $T = 160$ K ($\approx T_N + 24$ K), paramagnetic scattering is isotropic in spin space at all probed energies with $M_a = M_b = M_c$. At a temperature $T = 138$ K ($\approx T_N + 2$ K) slightly above

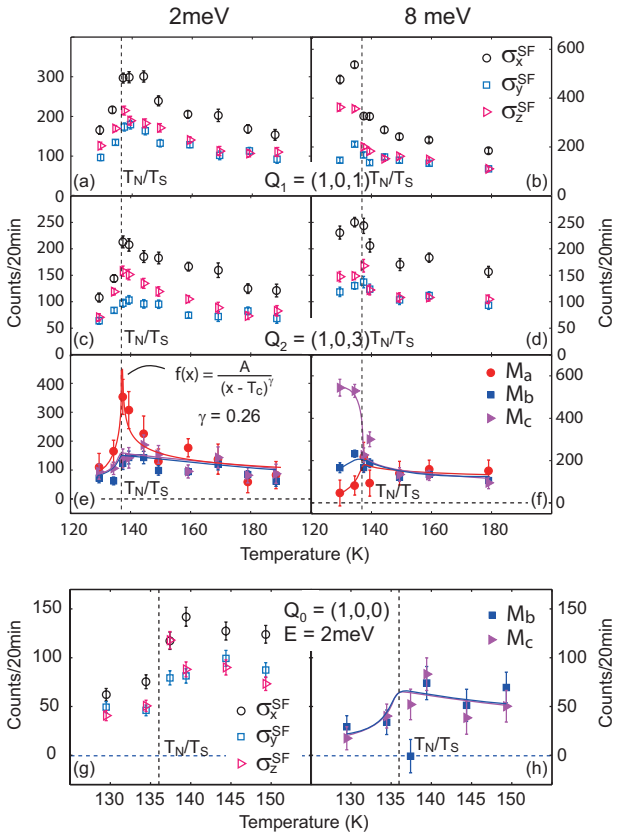

FIG. 4: (Color online) Temperature dependence of σ_x^{SF},σ_y^{SF}, and σ_z^{SF} at $E = 2$ meV with (a) $\mathbf{Q}_1 = (1, 0, 1)$ and (c) $\mathbf{Q}_2 = (1, 0, 3)$. Similar data at $E = 8$ meV with (b) $\mathbf{Q}_1 = (1, 0, 1)$ and (d) $\mathbf{Q}_2 = (1, 0, 3)$. (e) Temperature dependence of the components M_a, M_b, and M_c at $E = 2$ meV. The solid curve is the fitted line with function $f(T) = \frac{A}{(T-T_c)^\gamma}$. (f) Temperature dependence of M_a, M_b, and M_c at $E = 8$ meV. (g) The three SF scattering channels measured at $\mathbf{Q}_0 = (1, 0, 0)$ and $E = 2$ meV. (h) Temperature dependence of M_b and M_c determined from (g).The solid lines are guides to the eye. The vertical dashed lines mark T_N/T_s.

T_N, paramagnetic spin excitations are anisotropic below ~5 meV with $M_a > M_b \approx M_c$.

In previous unpolarized neutron scattering experiments on $BaFe_2As_2$ [9], two-dimensional (2D) magnetic critical scattering has been observed at temperatures far above T_N. Upon cooling, the longitudinal component of the critical scattering above T_N (M_a) is expected to increase with decreasing temperature and condense into the 3D AF Bragg positions at the 2D-3D dimensional crossover temperature T_{3D} near T_N [30]. The transverse components of spin excitations (M_b and M_c) are the spin wave contributions not expected to diverge at T_N [9]. To test if this is indeed the case, we measured temperature dependence of $\sigma_{x,y,z}^{SF}$ at $E = 2$ meV and 8 meV at the AF zone center $\mathbf{Q}_1$ [Figs. 4(a) and 4(b)] and $\mathbf{Q}_2$ [Figs. 4(c) and 4(d)]. With decreasing temperature, $\sigma_{x,y,z}^{SF}$ increases in intensity with the differences between σ_z^{SF} and σ_y^{SF} most obvious near T_N at $\mathbf{Q}_2$ [Fig. 4(c)]. Using data in Fig. 4(a) and 4(c), we estimate the temperature dependence of M_a, M_b, and M_c in Fig. 4(e). Consistent with the expectations from the magnetic critical scattering measurements [9], we see a diverging longitudinal spin excitations M_a at $E = 2$ meV while transverse spin excitations show no critical scattering around T_N. On cooling below T_N, all three polarizations of spin excitations are suppressed due to the formation of spin gaps [20]. Similar measurements at $E = 8$ meV show isotropic paramagnetic scattering behavior ($M_a \approx M_b \approx M_c$) down to T_N before splitting into $M_c > M_b > M_a$ seen in the AF ordered state [Fig. 4(f)]. Figure 4(g) shows temperature dependence of the spin excitations $\sigma_{x,y,z}^{SF}$ at $E = 2$ meV and zone boundary position $\mathbf{Q}_0$. We see that magnetic scattering is isotropic at all measured temperatures with no evidence of spin anisotropy.

The diverging M_a near T_N in $BaFe_2As_2$ may arise from the longitudinally polarized spin excitation in the critical scattering regime of a Heisenberg antiferromagnet with Ising spin anisotropy [Fig. 4] [33]. This means that the effect of critical scattering in $BaFe_2As_2$ can force the fluctuating moment along the longitudinal (a-axis) direction in the paramagnetic critical regime without the need for orthorhombic lattice distortion and associated ferro-orbital (nematic) ordering. Although this scenario is interesting, we note that temperature dependence of spin excitation anisotropy in the paramagnetic state of AF ordered NaFeAs [34] and electron underdoped $BaFe_{1.904}Ni_{0.096}As_2$ [15] behave differently. In previous polarized neutron scattering experiments on NaFeAs, which has a collinear AF order at $T_N = 45$ K and an orthorhombic-to-tetragonal lattice distortion at $T_s \approx 58$ K [31, 32], $M_a \approx M_c$ is larger than M_b in the paramagnetic orthorhombic phase below T_s and the in-plane anisotropy $M_a - M_b$ enhances on approaching T_N from T_s [34]. When warming up to above T_s, the statistics of the data in NaFeAs is insufficient to establish possible spin anisotropy [34]. Since one of the key differences between $BaFe_2As_2$ and NaFeAs is the coupled structural and magnetic phase transitions in $BaFe_2As_2$, our data suggest that the orthorhombic lattice distortion lifting the degeneracy of the Fe d_{xz} and d_{yz} orbitals also induces the M_c and M_b anisotropy. This is consistent with the observation that M_c has the lowest energy in spin waves of the AF ordered $BaFe_2As_2$ [20, 21] and NaFeAs [34], suggesting that it costs less energy for the a-axis ordered moment to rotate out of the plane than to rotate within the plane.

For electron doped $BaFe_{1.904}Ni_{0.096}As_2$ superconductor with $T_c = 19.8$ K and $T_N \approx T_s = 33 \pm 2$ K, spin excitation anisotropy at $E = 3$ meV and zone center $\mathbf{Q}_{AF}$ with $M_a \approx M_c > M_b$ first appears below ~70 K and shows no anomaly across T_s/T_N before changing dramatically below T_c [15]. For hole-doped $Ba_{0.67}K_{0.33}Fe_2As_2$ superconductor with $T_c = 38$ K and no structural/magnetic

order, spin excitation anisotropy at $E = 3$ meV and $\mathbf{Q}_{AF}$ with $M_a \approx M_c > M_b$ appears below ∼100 K, and also decreases abruptly T_c [19]. The similarities of these results to those of NaFeAs in the nematic temperature regime ($T_s > T > T_N$) suggest that the ferro-orbital order or fluctuations [35–40] in electron and hole-doped $BaFe_2As_2$ first appear in the paramagnetic tetragonal phase at temperatures well above T_s [15, 19]. Since SOC in iron pnictides is a single iron effect not expected to change dramatically as a function of electron and hole doping [41, 42], the weak/absence of M_c and M_b spin excitation anisotropy in the tetragonal phase of $BaFe_2As_2$ is difficult to understand. One possibility is that the nearly coupled structural and magnetic phase transitions in $BaFe_2As_2$ [8] suppress the role of the SOC induced ferro-orbital fluctuations above T_s. Although hole-doped $Ba_{1-x}K_xFe_2As_2$ also has coupled structural and magnetic phase transitions in the underdoped regime [22], it changes to a double-$\mathbf{Q}$ tetragonal magnetic structure with ordered moments along the c-axis near optimal superconductivity [23–25]. When hole and electron doping in $BaFe_2As_2$ reduces the structural and magnetic ordering temperatures, the SOC induced ferro-orbital fluctuations start to appear at temperatures above T_s. In this picture, the spin excitation anisotropy in the superconducting iron pnictides originates from similar anisotropy already present in their parent compounds below T_s. The dramatic change in spin excitation anisotropy across T_c seen in electron and hole-doped $BaFe_2As_2$ suggests a direct coupling of the SOC to superconductivity. The systematic polarized neutron scattering measurements present here and in previous work on doped $BaFe_2As_2$ family of materials [13–19] call for quantitative calculations on how SOC is associated with spin excitation anisotropy in iron pnictides.

The neutron scattering work at Rice is supported by the U.S. NSF-DMR-1436006 and NSF-DMR-1362219 (P.D.). The materials synthesis efforts at Rice are supported by the Robert A. Welch Foundation Grant No. C-1839 (P.D.).

* Electronic address: pdai@rice.edu

[1] H. Hosono and K. Kuroki, Physica C, **514**, 399-422 (2015).
[2] G. R. Stewart, Rev. Mod. Phys. **83**, 1589-1652 (2011).
[3] P. C. Dai, Rev. Mod. Phys. **87**, 855 (2015).
[4] I. R. Fisher, L. Degiorgi, and Z. X. Shen, Rep. Prog. Phys. **74**, 124506 (2011).
[5] R. M. Fernandes, A. V. Chubukov, J. Schmalian, Nat. Phys. **10**, 97-104 (2014).
[6] A. E. Böhmer, C. Meingast, C. R. Physique **17** 90-112 (2016).
[7] Q. Huang, Y. Qiu, Wei Bao, M. A. Green, J. W. Lynn, Y. C. Gasparovic, T. Wu, G. Wu, X. H. Chen, Phys. Rev. Lett. **101**, 257003 (2008).
[8] M. G. Kim, R. M. Fernandes, A. Kreyssig, J. W. Kim, A. Thaler, S. L. Bud'ko, P. C. Canfield, R. J. McQueeney, J. Schmalian, A. I. Goldman, Phys. Rev. B **83**, 134522 (2011).
[9] S. D. Wilson, Z. Yamani, C. R. Rotundu, B. Freelon, P. N. Valdivia, E. Bourret-Courchesne, J. W. Lynn, Songxue Chi, Tao Hong, and R. J. Birgeneau, Phys. Rev. B **82**, 144502 (2010).
[10] S. V. Borisenko, D. V. Evtushinsky, Z.-H. Liu, I. Morozov, R. Kappenberger, S. Wurmehl, B. Bühner, A. N. Yaresko, T. K. Kim, M. Hoesch, T. Wolf, and N. D. Zhigadlo, Nat. Phys. **12**, 311 (2016).
[11] R. M. Fernandes, A. V. Chubukov, J. Knolle, I. Eremin, and J. Schmalian, Phys. Rev. B **85**, 024534 (2012).
[12] Hsueh-Hui Kuo, Jiun-Haw Chu, Johanna C. Palmstrom, Steven A. Kivelson, Ian R. Fisher, Science **352**, 958 (2016).
[13] O. J. Lipscombe, Leland W. Harriger, P. G. Freeman, M. Enderle, Chenglin Zhang, Miaoying Wang, Takeshi Egami, Jiangping Hu, Tao Xiang, M. R. Norman, and Pengcheng Dai, Phys. Rev. B **82**, 064515 (2010).
[14] P. Steffens, C. H. Lee, N. Qureshi, K. Kihou, A. Iyo, H. Eisaki, and M. Braden, Phys. Rev. Lett. **110**, 137001 (2013).
[15] Huiqian Luo, Meng Wang, Chenglin Zhang, Xingye Lu, Louis-Pierre Regnault, Rui Zhang, Shiliang Li, Jiangping Hu, and Pengcheng Dai, Phys. Rev. Lett. **111**, 107006 (2013).
[16] F. Waβer, C. H. Lee, K. Kihou, P. Steffens, K. Schmalzl, N. Qureshi, and M. Braden, arXiv: 1609.02027V1.
[17] Chenglin Zhang, Mengshu Liu, Yixi Su, Louis-Pierre Regnault, Meng Wang, Guotai Tan, Th. Brückel, Takeshi Egami, and Pengcheng Dai, Phys. Rev. B **87**, 081101 (2013).
[18] N. Qureshi, C. H. Lee, K. Kihou, K. Schmalzl, P. Steffens, and M. Braden, Phys. Rev. B **90**, 100502 (2014).
[19] Y. Song, H. R. Man, R. Zhang, X. Y. Lu, C. L. Zhang, M. Wang, G. T. Tan, L.-P. Regnault, Y. X. Su, J. Kang, R. M. Fernandes, and P. C. Dai, Phys. Rev. B **94**, 214516 (2016).
[20] N. Qureshi, P. Steffens, S. Wurmehl, S. Aswartham, B. Büchner, and M. Braden, Phys. Rev. B **86**, 060410(R) (2012).
[21] Chong Wang, Rui Zhang, Fa Wang, Huiqian Luo, L. P. Regnault, Pengcheng Dai, and Yuan Li, Phys. Rev. X **3**, 041036 (2013).
[22] S. Avci, O. Chmaissem, D. Y. Chung, S. Rosenkranz, E. A. Goremychkin, J. P. Castellan, I. S. Todorov, J. A. Schlueter, H. Claus, A. Daoud-Aladine, D. D. Khalyavin, M. G. Kanatzidis, and R. Osborn Phys. Rev. B **85**, 184507 (2012).
[23] S. Avci, O. Chmaissem, J. M. Allred, S. Rosenkranz, I. Eremin, A. V. Chubukov, D. E. Bugaris, D. Y. Chung, M. G. Kanatzidis, J.-P Castellan, J. A. Schlueter, H. Claus, D. D. Khalyavin, P. Manuel, A. Daoud-Aladine, and R. Osborn, Nat. Commun. **5**, 3845 (2014).
[24] F. Waβer, A. Schneidewind, Y. Sidis, S. Wurmehl, S. Aswartham, B. Buchner, and M. Braden, Phys. Rev. B **91**, 060505 (2015).
[25] J. M. Allred, K. M. Taddei, D. E. Bugaris, M. J. Krogstad, S. H. Lapidus, D. Y. Chung, H. Claus, M. G. Kanatzidis, D. E. Brown, J. Kang, R. M. Fernandes, I. Eremin, S. Rosenkranz, O. Chmaissem, and R. Osborn, Nat. Phys. **12**, 493 (2016).

[26] Haoran Man, Xingye Lu, Justin S. Chen, Rui Zhang, Wenliang Zhang, Huiqian Luo, J. Kulda, A. Ivanov, T. Keller, Emilia Morosan, Qimiao Si, and Pengcheng Dai. Phys. Rev. B **92**, 134521 (2015).

[27] D. M. Pajerowski, C. R. Rotundu, J. W. Lynn, and R. J. Birgeneau, Phys. Rev. B **87**, 134507 (2013).

[28] Yu Song, Louis-Pierre Regnault, Chenglin Zhang, Guotai Tan, Scott V. Carr, Songxue Chi, A.D. Christianson, Tao Xiang, and Pengcheng Dai, Phys. Rev. B **88**, 134512 (2013).

[29] Chenglin Zhang, Yu Song, L.-P. Regnault, Yixi Su, M. Enderle, J. Kulda, Guotai Tan, Zachary C. Sims, Takeshi Egami, Qimiao Si, and Pengcheng Dai, Phys. Rev. B **90**, 140502 (2014).

[30] S. D. Wilson, Z. Yamani, C. R. Rotundu, B. Freelon, E. Bourret-Courchesne, and R. J. Birgeneau, Phys. Rev. B **79**, 184519 (2009).

[31] Dinah R. Parker, Michael J. Pitcher, Peter J. Baker, Isabel Franke, Tom Lancaster, Stephen J. Blundell, and Simon J. Clarke, Chem. Commun. (Cambridge) (2009) 2189.

[32] S. Li, C. de la Cruz, Q. Huang, G. G. Chen, T.-L. Xia, J. L. Luo, N. L. Wang, and P. C. Dai, Phys. Rev. B **80**, 020504(R) (2009).

[33] M. F. Collin, *Magnetic Critical Scattering* (Oxford University Press, New York, 1989), Chapter 8.

[34] Y. Song, L. P. Regnault, C. L. Zhang, G. T. Tan, S. V. Carr, S. X. Chi, A. D. Christianson, T. Xiang, and P. C. Dai, Phys. Rev. B **88**, 134512 (2013).

[35] R. M. Fernandes, A. V. Chubukov, J. Knolle, I. Eremin, and J. Schmalian, Phys. Rev. B **85**, 024534 (2012).

[36] C. C. Lee, W. G. Yin, and W. Ku, Phys. Rev. Lett. **103**, 267001 (2009).

[37] F. Krüger, S. Kumar, J. Zaanen, and J. van den Brink, Phys. Rev. B **79**, 054504 (2009).

[38] W. C. Lv, J. S. Wu, and P. Phillips, Phys. Rev. B **80**, 224506 (2009).

[39] C.-C. Chen, , J. Maciejko, A. P. Sorini, B. Moritz, R. R. P. Singh, and T. P. Devereaux, Phys. Rev. B **82**, 100504(R) (2010).

[40] B. Valenzuela, E. Bascones, and M. J. Calderón, Phys. Rev. Lett. **105**, 207202 (2010).

[41] V. Cvetkovic and O. Vafek, Phys. Rev. B **88**, 134510 (2013).

[42] R. M. Fernandes and O. Vafek, Phys. Rev. B **90**, 214514 (2014).